Theoretical calculations of the Xe chemical shifts in cryptophane cages

Devin N. Sears and Cynthia J. Jameson[a)]
Department of Chemistry, M/C-1 11, University of Illinois at Chicago, Chicago, Illinois 60607-7061

(Received 21 August 2003; accepted 22 September 2003)

Toward an understanding of the factors that affect the chemical shift in the Xe nuclear magnetic resonance spectrum of Xe atoms trapped in cages which may have applications as biosensors, we carry out calculations of Xe nuclear magnetic shielding using Hartree–Fock and density functional methods. The resulting values for various Xe positions within the cage can be described by an analytical function of Xe and cage atom coordinates. This shielding function is used in Monte Carlo canonical averaging of a Xe atom within cryptophane cages to investigate the dependence of the Xe chemical shifts on cage size (cryptophane-A versus cryptophane-E), isotopic substitution, and temperature. We compare our theoretical average Xe chemical shifts with the experimental values in four types of cryptophane cages, and with the temperature and isotopic dependence of Xe chemical shifts in cryptophane-A, and achieve a quantitative understanding of the factors that influence the Xe chemical shifts in these cages. The predicted effects on the Xe chemical shifts of mechanical distortion of the cryptophane-A cage provide some insight into the applications of Xe in cages as biosensors. © *2003 American Institute of Physics.* [DOI: 10.1063/1.1625364]

I. INTRODUCTION

The affinity of Xe for hydrophobic cavities in macromolecular interiors has motivated a variety of applications of this inert gas in biochemical and structural studies in proteins,[1–4] in cells,[5,6] and in tissues.[7–9] Rubin *et al.* have been developing ^{129}Xe nuclear magnetic resonance (NMR) as a tool for detecting protein cavities that bind xenon and using Xe chemical shifts as a reporter of cavity structure in proteins in solution, as well as in crystals.[10] Comparison between native and cavity mutants of the same protein suggests that smaller cavities give rise to larger Xe deshielding than larger cavities. This finding is consistent with the general correlation of greater Xe deshielding with decreasing cavity size in clathrate hydrates[11] and in zeolites.[12,13]

Xenon atoms in cages of various types have exhibited intermolecular NMR chemical shifts over a wide range of values. Some notable examples are Xe in small and large cages of clathrate hydrates Structure I and Structure II in which the chemical shifts are, respectively, 242, 152, 225, and 80 ppm.[11,14–16] In the alpha cages of zeolite NaA, the Xe chemical shifts range from 75 to 272 ppm.[17] In the organic cage of cryptophane-A the Xe chemical shift is 63 ppm,[18] while in the somewhat larger cage of the same type, cryptophane-E, it is 30 ppm smaller.[19] The exquisite sensitivity of the xenon chemical shift to its environment has motivated the development of Xe inserted into functionalized cryptophane cages as biosensors for proteins in solution.[19]

An understanding of the Xe chemical shifts which provide the biosensor capability would be useful, especially for the multiplexing scheme (many different cages recognizing many different proteins, all in the same solution) that is desired. It is beyond our present capability to calculate Xe chemical shifts in a cryptophane cage functionalized with a long tether, before and after binding to the protein. On the other hand, predictions of caged Xe shifts for this application require a quantitative understanding of the sensitivity of the isotropic Xe chemical shift in various cryptophane cages. Fortunately, there are experimental data with which to test calculations of average Xe chemical shifts in the parent cryptophane cages, in particular the observed dependence on cage size, isotopic substitution, and temperature. We require a quantum mechanical description of the Xe shielding response to a cryptophane cage and a statistical mechanical averaging over the possible Xe configurations within the cage. In this paper, we investigate these effects and demonstrate that it is possible to have a quantitative understanding of the Xe chemical shifts in these simpler cages, including the dependence on cage size, temperature, and isotopic substitution. From this properly tested approach, we attempt computer simulations that permit us to comment on Xe chemical shifts in biosensor systems.

II. METHODS

A. Determination of the cage geometry in solution

The chemical formula of the cryptophane-A cage, which is chiral, is shown in Fig. 1. The OCH_3 groups display an *anti*relationship with respect to the bridges, whereas the *syn* isomer is cryptophane-B, (not yet isolated) which is achiral.[20] The x-ray structure of crystalline cryptophane-A was generously provided to us by Professor Dutasta prior to publication.[21] However, this structure is not exactly what we are looking for. First, the geometry of the cage in the solid state corresponds to a lower symmetry than the cage would

a)Author to whom correspondence should be addressed; electronic mail: cjjames@uic.edu

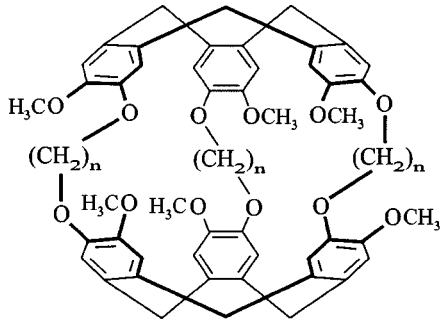

Two cyclotriveratrylene bowls connected by aliphatic linkers $(CH_2)_n$

n = 2,2,2 cryptophane-A
n = 3,3,3 cryptophane-E
n = 2,2,3 cryptophane-223
n = 2,3,3 cryptophane-233

FIG. 1. Chemical formulas of cryptophane cages.

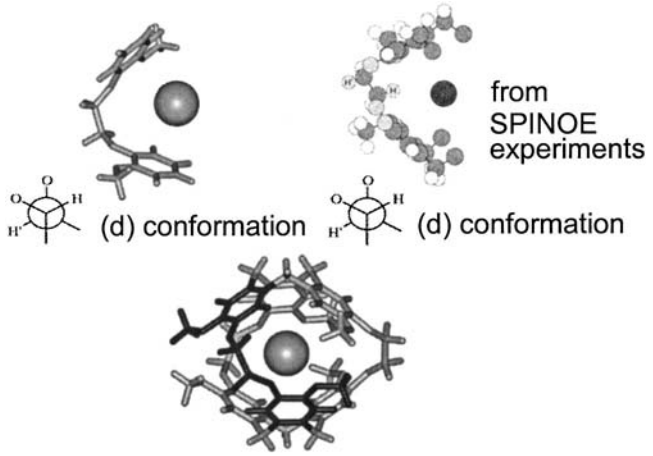

FIG. 2. The OCH_2CH_2O groups have a gauche conformation in the quantum-mechanically optimized structure for cryptophane-A. The minimum energy structure arrived at is consistent with SPINOE experiments by Pines *et al.* The proposed structure in Ref. 24 is reproduced, with permission from the American Chemical Society.

have in solution. Crystal packing forces lead to a cryptophane-A cage molecule with C_1 symmetry in its lattice site, with the three OCH_2CH_2O linkers being nonequivalent, and the six rings and OCH_3 groups likewise nonequivalent. The six capping CH_2 groups are also nonequivalent. Equivalence of these groups for the molecule in solution would lead to D_3 symmetry. Therefore, we need to symmetrize the structure of the molecule starting from the known structure in the crystal. Second, the structure of an empty cage is not necessarily the same as the structure of the cage containing a Xe atom. For example, molecular dynamics simulations by Varnek *et al.*[22] on cryptophane-E with and without tetrahedral guests reveal that, in the absence of a guest, the cavity tends to be filled by its own bridging propylene and methoxy fragments in the gas phase simulations. In $CHCl_3$ solution, on the other hand, these molecular dynamics simulations find the cavity filled with a $CHCl_3$ molecule and the methoxy and bridging groups therefore have different geometries than in the gas phase simulations. The degrees of freedom associated with the OCH_2CH_2O linkers in cryptophane-A allow the molecule to adopt various conformations. These conformations involve changes in the dihedral angles. The conformation of the linker can be anti (referring to the bonds to the O atoms having a 180° dihedral angle) of which there are two possibilities, or gauche (a 60° dihedral angle), of which there are two possibilities. In particular, the conformations of the linkers in the crystalline state have been found to be mixed anti and gauche,[21] and in solution, the linkers are known to have all the same conformation, giving rise to D_3 symmetry, but unknown as to anti or gauche.[23] On the other hand the SPINOE studies of Pines and co-workers led to the conclusion that the cryptophane-A cage containing a Xe atom is most consistent with the structure shown in Fig. 2, i.e., the OCH_2CH_2O groups have a gauche conformation, of the type which they labeled (d).[24] The SPINOE experiments are found to be inconsistent with the anti–anti–anticonformation of the linkers. With the Xe atom occupying some of the internal volume of the cage, the linkers are apparently unable to assume the anti–anti–anticonformation.

We found the minimum energy structure of the cryptophane-A cage by the method shown schematically in Fig. 3. First, the average bond lengths and angles of the cyclotriveratrylene bowl are taken from the x-ray diffraction structure.[21] The C_3 symmetry operations generate the starting structure for the cyclotriveratrylene bowl. We then use quantum mechanical geometry optimization to find the minimum energy arrangements (C_{ring}–O–C bond angles and bond lengths, and orientation relative to the plane of the aromatic ring) of the OCH_3 groups for the half cage. This set of atomic coordinates for the cyclotriveratrylene bowl is used for the quantum mechanical shielding calculations and forms the basis for generating the full cage structure.

We now introduce the OCH_2CH_2O conformations. Since the system is too large to do this conveniently quantum mechanically for the full cage, only one third of the cage is used, that is, the fragment shown in Fig. 3, together with the Xe atom at the origin (center of the cage). With the capping methylenes converted to hydrogens, and retaining the pole-to-pole distance and the bowl-to-bowl twist found in the crystal diffraction structure, we have a starting point for optimization of one third of the cage. The Xe and ring atoms are fixed and geometry optimization was carried out using the density functional method (with the B3LYP functional). Starting with small basis sets (STO-3G) and the anticonformation, we find that the cage fragment with the Xe atom ends up in the (d) gauche conformation, and retains the specific (d) gauche conformation upon every step of the geometry optimization, through increasing basis set size, up to the basis set (240 basis functions on Xe atom and 6-311G** for the rest of the atoms) to be used for the Xe nuclear magnetic shielding calculations. The optimum conformation found is in complete agreement with the SPINOE experiments of Luhmer *et al.*[24] In order to find the complete structure of the

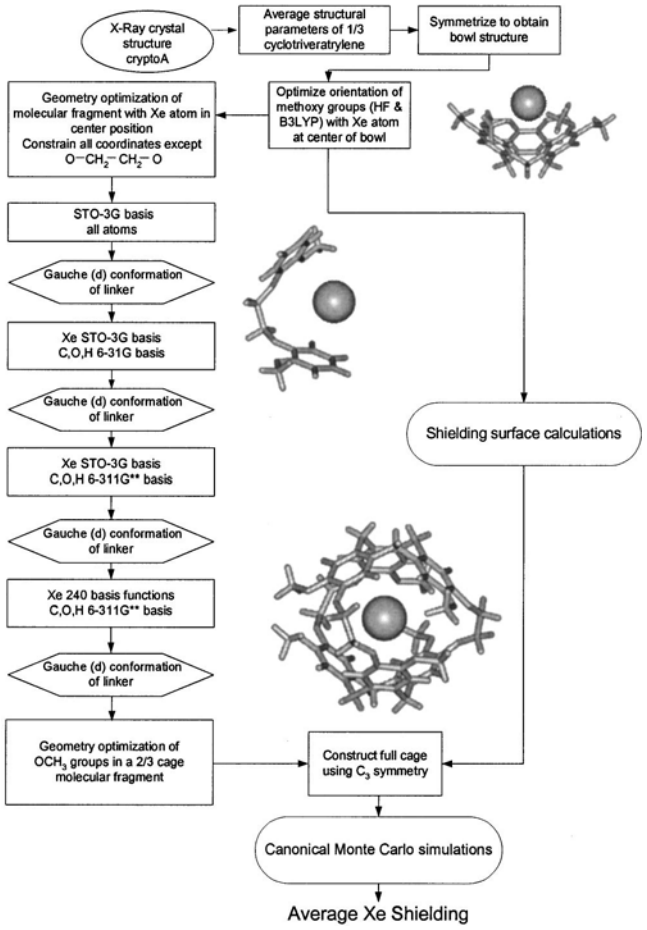

FIG. 3. Schematic diagram of the method of determination of the structure of cryptophane-A in solution.

cage, we then constructed a fragment which is 2/3 of the cage, in which the two rings at each pole are connected via a capping methylene. Retaining the (d) gauche conformation of the linkers, we again carried out DFT/B3LYP geometry optimization to permit the OCH_3 groups to find their optimum position in the cage with the Xe atom. The resulting optimum geometry for the 2/3 fragment is used to generate the full cage. This is our optimum static representation of the average cryptophane-A cage structure in solution.

With the additional CH_2 group in each of the three linkers, cryptophane-E is a larger cage than cryptophane-A. The x-ray diffraction structure of crystalline cryptophane-E (complexed with $CHCl_3$)[25] reveals nearly D_3 symmetry for the cage and each of the three $O(CH_2)_3O$ bridges has about the same conformation, with the pseudo C_2 axes passing through the inner methylenes of the chains. The methoxy groups show some orientational disorder. Since the coordinates of the cyclotriveratrylene bowl (except for the OCH_3 groups) in cryptophane-E are consistent with those in cryptophane-A, we start with these atomic coordinates as optimized, and only the conformation of the $OCH_2CH_2CH_2O$ linkers and the coordinates of the OCH_3 groups need to be found. We find the best static representation of the structure of cryptophane-E in solution by using the same geometry optimization strategy as we used for cryptophane-A: the linker conformation is found by using 1/3 of the cage, then the coordinates of the OCH_3 groups are found by using 2/3 of the cage with the Xe atom at the cage center. All six methoxy groups are equivalent in our quantum-mechanically optimized structure for cryptophane-E containing a Xe atom. With the quantum-mechanical geometry optimization described here, we find the coordinates for the atoms of cryptophane-E. This structure is consistent with the conformation of the $O(CH_2)_3O$ linkers of crystalline cryptophane-E (complexed with $CHCl_3$).[25]

B. *Ab initio* calculations of the shielding values of Xe at the cyclotriveratrylene bowl

For the calculations of the average Xe chemical shift, we need a large number of Xe shielding values at arbitrary positions within the cage. The full cage of cryptophane-A together with the Xe atom is too large a system for *ab initio* shielding calculations of the required number. Thus, we used Xe in half the cryptophane cage, a cyclotriveratrylene bowl. Only the coordinates of the OCH_3 groups needed to be quantum mechanically optimized. We will assume Xe shielding contributions from the top and bottom halves of the cage to be additive.

All quantum-mechanical shielding calculations were carried out using the gauge-including atomic orbitals choice of distributed origins.[26] The Xe basis set of 240 functions that we have used in previous work,[27,28] and 6-311G** basis set for the remaining atoms constitute 1014 basis functions for Xe and the cyclotriveratrylene bowl. The quality of the Xe basis set we are using leads to a very small counterpoise correction to the shielding response. For the DFT/B3LYP calculations, the difference in shieldings calculated for the free Xe atom using only the 240 basis functions of Xe and that using the entire 1014 basis functions amounts to only 0.01 ppm.

Unique (not symmetry-related) positions for the Xe atom were chosen along various approaches toward the bowl face. We compare the results of Hartree–Fock calculations of Xe shielding with DFT/B3LYP calculations in Fig. 4. The Hartree–Fock (HF) method leaves out the electron correlation contributions to shielding while providing exact exchange. The density functional theory (DFT) method does include electron correlation but uses an empiricized combination of exchange and correlation functional. In our other work in Xe shielding calculations where direct comparison with gas phase results can serve as tests, the experimental shielding is found to lie between the predictions from the two methods with experimental values being reproduced by 1.16 times the HF shielding function or 0.85 times the B3LYP shielding function.[28] We anticipate similar differences between the HF and B3LYP results in the cryptophane case. Furthermore, we expect additional deficiencies in using the Hartree–Fock method for the Xe shielding calculations when the neighboring molecule explicitly requires electron correlation for a reasonable description of its electronic

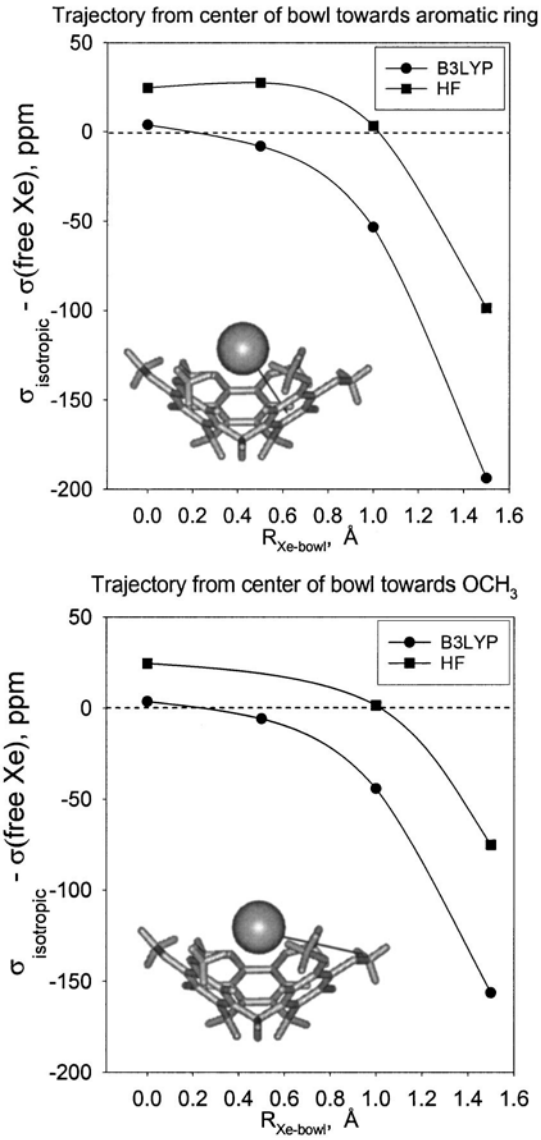

FIG. 4. Results of calculations of isotropic Xe shielding for Xe atom at various positions in the cyclotriveratrylene bowl, using Hartree–Fock and DFT/B3LYP methods.

structure. We have found that Hartree–Fock calculations are particularly deficient where the Xe shielding response to aromatic rings is concerned.[29] The Xe shielding predicted by Hartree–Fock in most of the regions of interest (in the vicinity of the center of the cage) is greater than that of the free Xe atom. Thus, the Hartree–Fock shielding response for Xe would lead to an average Xe chemical shift that would have the wrong sign relative to the free Xe atom. Therefore, we choose the shielding results from the DFT method, while expecting that we may find somewhat overestimated deshielding in our calculated values, based on our results with the Xe–rare gas pairs.[28]

A total of 25 unique Xe positions were used for the shielding calculations in and above the half cage, along various directions of approach toward the cage atoms. Symmetry operations generate 75 positions, thereby providing sufficient exploration of the space within the bowl. We will use these shielding calculations as the basis for calculating the average shielding response of Xe in both cryptophane-A and cryptophane-E, and in two other cryptophane cages with lower symmetry.

C. Description of the shielding surface for Xe in cryptophane-A

In order to be able to find the isotropic Xe shielding at an arbitrary location inside the cage of cryptophane-A (and cryptophane-E), we describe the isotropic Xe shielding response as a sum of atomic contributions. We find a theoretical shielding surface that is expressed as a sum over five Xe-site shielding functions. The five types of sites correspond to: C_{ring}, C_{CO}, C_{cap}, O, and O_{lp}. The C_{cap} sites are the CH_2 groups linking the aromatic rings together. The C_{CO} sites are the carbon atoms in the OCH_2CH_2O linkers. The CH_3 groups attached to O atoms are assumed to be the same type of site. The C_{ring} sites represent the aromatic ring carbons. Contributions to the Xe shielding from hydrogen atoms are not separated out. They are subsumed in the carbon sites they are attached to. Each oxygen atom is represented by a site (O) at the oxygen center and a site (O_{lp}) representing the centroid of the lone pairs 1.2 Å from the oxygen center. The need for including a lone pair site became obvious from the significant deshielding values found for Xe above the bowl.

Smooth curves were drawn through the DFT/B3LYP values for the various Xe positions and values of isotropic Xe shielding were interpolated. The interpolated values were found necessary to keep the fitted functions from adopting oscillatory behavior between the original Xe positions. In the fitting procedure, each of the five site-shielding functions is constrained to be properly behaved in the limit of large separations, i.e., each function should approach the shielding of the free Xe atom in this limit. Upon closer approach to each site, the Xe-site shielding response is assumed to become monotonically more deshielding, which is the behavior of the Xe shielding response when the Xe atom is interacting with other rare gas atoms, at least up to a separation of $0.6r_0$, well before the minimum in the shielding function is reached.[28] We believe this to be the universal behavior of the Xe intermolecular shielding response, that is, the same limiting behavior of Xe shielding response found for the Xe atom interacting with small molecules such as CO_2, N_2, CO, and Xe–rare gas pairs.[27,28] As an exception, positive shielding was permitted for the ring carbon sites to take into account the *ab initio* results showing positive values in a small region where ring currents would predict shielding rather than deshielding. Using these Xe-site shielding functions, the quantum mechanical values of Xe shielding calculated at various positions within the cage can be reconstituted, and the Xe shielding response at arbitrary positions within the cage A (and also within cage E and other hybrid cages between A and E types) can be calculated as follows:

$$\sigma_{\mathrm{iso}}(\mathbf{r})=\sum_{i}^{O} a_6[r(\mathrm{Xe–O}_i)]^{-6}+a_8[r(\mathrm{Xe–O}_i)]^{-8}+\ldots+a_{12}[r(\mathrm{Xe–O}_i)]^{-12}$$
$$+\sum_{i}^{\mathrm{lp}} b_6[r(\mathrm{Xe–lp}_i)]^{-6}+b_8[r(\mathrm{Xe–lp}_i)]^{-8}+\ldots+b_{12}[r(\mathrm{Xe–lp}_i)]^{-12}$$
$$+\sum_{k}^{\mathrm{ring}} c_6[r(\mathrm{Xe–C}_k)]^{-6}+c_8[r(\mathrm{Xe–C}_k)]^{-8}+\ldots+c_{12}[r(\mathrm{Xe–C}_k)]^{-12}$$
$$+\sum_{n}^{\mathrm{cap}} d_6[r(\mathrm{Xe–C}_n)]^{-6}+d_8[r(\mathrm{Xe–C}_n)]^{-8}+\ldots+d_{12}[r(\mathrm{Xe–C}_n)]^{-12}$$
$$+\sum_{j}^{\mathrm{C–O}} e_6[r(\mathrm{Xe–C}_j)]^{-6}+e_8[r(\mathrm{Xe–C}_j)]^{-8}+\ldots+e_{12}[r(\mathrm{Xe–C}_j)]^{-12}. \quad (1)$$

The above equation is appropriately viewed as an interpolating function that permits us to reproduce the Xe shielding values at those points where they are known from the quantum-mechanical calculations, and to estimate the expected shielding values at arbitrary points between these known ones.

D. Monte Carlo simulations

Canonical Monte Carlo simulations were carried out using the site shielding functions developed above. For Xe–ring interactions, we used the Xe–benzene potential function from Brupbacher *et al.*[30] This Xe@ benzene potential function is of the form

$$V=V_0\left\{\sum_i u^2(R_i)+w\sum_{i>j} u(R_i)u(R_j)\right\}, \quad (2)$$

where the summation over i and j is over the six carbons in benzene. The function u was chosen in such a way as to reproduce for $w=0$ the usual Lennard-Jones 6–12 form, i.e.,

$$u(R_i)=[1-(R_0/R_i)^6], \quad (3)$$

where R_0 is related to the equilibrium distance R_e between the Xe and the center of mass of benzene as follows:

$$R_e=[R_0^2-R_{\mathrm{CC}}^2]^{1/2}, \quad (4)$$

in which R_{CC} is the carbon–carbon bond length in benzene. The hydrogens are not considered explicitly; their effect is considered implicitly in the carbon parameters. The three adjustable parameters of this potential, V_0, w, and R_e, were fitted to the observed rotational transition frequencies of the Xe–benzene van der Waals complex.[30] The parameters used in our work were taken directly from Ref. 30.

For Xe–CH_n interactions (cap, linker, and methoxy groups), we used the same potential function as for Xe–CH_4.[31] This is a site–site pairwise additive function

$$V(\mathrm{Xe–CH_4})=V(r_{\mathrm{XeC}})+\sum_i V(r_{\mathrm{XeHi}}), \quad (5)$$

where $V(\mathrm{r_{XeC}})$ and $V(\mathrm{r_{XeHi}})$ are taken to be of the Maitland–Smith form[32]

$$V=\epsilon\{(6/n-6)\bar{r}^{-n}-(n/n-6)\bar{r}^{-6}\}, \quad (6)$$

where n is allowed to vary with $\bar{r}=r/r_{\min}$ according to $n=m+\gamma(\bar{r}-1)$. We use the parameters found in Ref. 31 by fitting to the best available empirical potential function[33] for Xe–CH_4, a Morse–spline–van der Waals form that reproduced the absolute values of the integral cross sections and the glory extrema positions from molecular beam scattering experiments.

For the Xe–O potential we used a Maitland–Smith function starting from the Xe–Ne parameters, namely $m=13$, $\gamma=5$, $\epsilon/k=65.42$ K, $r_{\min}=3.924$ Å,[32] increasing the well depth and decreasing the $r_{\min}$ to the final set of Xe–O parameters: $\epsilon/k=65.42$ K, $r_{\min}=3.824$ Å. As expected, the $r_{\min}$ is somewhat longer and the well depth is somewhat smaller than the Xe–O parameters for the Xe–OH_2 potential functions in clathrate hydrate cages.[34] The simulation box was the cage itself. For efficiency, Xe was not permitted outside a radius of 5.0 Å from the center of the cage. A summary of the potential parameters used in this work is given in Table I.

E. Molecular dynamics simulations

Molecular mechanics molecular dynamics (MD) simulations were carried out to find optimum cage geometries for cages with mixed linker groups (223 and 233, as seen in Fig. 1), since x-ray data were not available for these cryptophanes. For these simulations the program package *CERIUS*^{2} (MSI, San Diego) was used, with the CVF91 force field parameters. The latter is the best force field available in this software package for compounds of this type. The potential cutoffs for both the van der Waals and Coulombic terms were set at 14 Å, implementing a nearest neighbor list. First, the liquid solvent $(CHCl_2)_2$ is equilibrated to the experimental density at room temperature (120 molecules in a 20 970 Å^3 box) using simulated annealing. Five solvent molecules are removed and replaced by the solute, a guest-filled-cryptophane cage. The liquid was permitted to relax after introduction of the solute. Molecular dynamics simulations consisting of three 5 ps trajectories were run at 100, 200, and 300 K, followed by a 10 ps trajectory at 300 K. 2 fs time

TABLE I. Potential parameters used in this work.

Maitland–Smith	$V=\epsilon\{(6/n-6)\bar{r}^{-n}-(n/n-6)\bar{r}^{-6}\}$		$\bar{r}=r/r_{\min}$	$n=m+\gamma(\bar{r}-1)$
	m	γ	$r_{\min}$ (Å)	ϵ/k (K)
Xe–C[a]	13	5	4.0047	141.52
Xe–H[a]	13	9.5	3.671	53.07
Xe–O[b]	13	5	3.824	65.42
Xe–ring[c]	$V=V_0\{\Sigma_i u^2(R_i)+w\Sigma_{i>j}u(R_i)u(R_j)\}$		$u(R_i)=[1-(R_0/R_i)^6]$	$R_e=[R_0^2-R_{CC}^2]^{1/2}$
		w	R_e (Å)	V_0 (K)
		−0.1509	3.7714	244.596

[a]Adopted from the $V(\mathrm{Xe}-\mathrm{CH_4})$ function (Ref. 31) that is the best fit to Liuti *et al.* (Ref. 33).
[b]This work.
[c]Adopted from V(Xe–benzene) from Ref. 30.

steps were used in all simulations. This serves as a suitable starting point for a steepest descent determination of the minimum energy structure in solution.

We used three guest molecules: CH_4 was somewhat too small compared to Xe; CCl_4 was somewhat too large; $CHCl_3$ was just the right size. Cryptophane-A and -E were used to test whether the force field used for the intermediate cryptophanes was adequate. The minimum energy structure arrived at for cryptophane-A with encapsulated $CHCl_3$ in $(CHCl_2)_2$ solvent was in good agreement with the quantum-mechanically optimized equilibrium structure of cryptophane-A with encapsulated Xe in vacuum. With $CHCl_3$ as guest, the molecular mechanics MD results for cryptophane-E in the same solvent produced a minimum energy structure that is likewise in good agreement with the quantum-mechanically optimized structure of cryptophane-E with encapsulated Xe.

With the MD procedure using the CVF91 force fields having been calibrated by the quantum-mechanically optimized Xe containing structures for the two symmetrical cages (cryptophane-A is the 222 cage, cryptophane-E is the 333 cage), the minimum energy structures for the hybrid 223 and 233 cages containing $CHCl_3$ can be expected to be equally reliable. The MD simulations are also used to generate the transient distorted cages that provide a measure of the range of cage deformation that occurs in solution.

III. RESULTS

In the SPINOE experiments of Luhmer *et al.* on Xe in cryptophane-A in $(CDCl_2)_2$ at room temperature,[24] both of the all-*anti*conformations were found to be inconsistent with the experimental H–Xe cross-relaxation rates for the protons of the linkers (relative to the values for the aromatic protons). Both gauche structures lead to relative $\langle r_{\mathrm{XeH}}^{-6}\rangle$ values for the linker protons in good agreement with experimental results, with the calculated $\langle r_{\mathrm{XeH}}^{-6}\rangle$ values for the (d) conformation more closely reproducing the experimental values. As seen in Fig. 2, the quantum-mechanically optimized structure (in vacuum) for a cryptophane-A cage containing a Xe atom in the present work is completely consistent with the SPINOE experiments of Pines *et al.* [i.e., the particular gauche conformation they designated as the (d) conformation] for all three linkers.

Whereas the cryptophane-A x-ray structure showed a much distorted cage, the cryptophane-E in the crystal is closer to the correct symmetry in solution. The quantum-mechanically optimized structure of the cryptophane-E cage containing a Xe atom in vacuum that we arrived at is consistent with that found in the x-ray diffraction in the solid[25] with respect to the geometry of the methoxy groups and the conformations of the linkers.

The shielding surface for Xe inside the cryptophane-A cage is illustrated in part in Fig. 5, where the isotropic shielding values are shown (relative to the free Xe atom) for those Xe locations in the plane of the equator of the A cage. Note that the Xe shielding in the center of the cage is a small positive shielding and becomes large negative shielding as Xe approaches the cage atoms. Note also the threefold symmetry of the bowl is reflected in the shielding surface. This is a necessary consequence and advantage of the additive form assumed in Eq. (1).

We used the isotropic Xe-site shielding functions and the Xe-site potential functions in obtaining the average Xe chemical shifts. The experimental chemical shift δ is related to the shielding σ as follows:

$$\langle\delta(\mathrm{Xe@cage})\rangle=[\sigma(\text{free Xe atom})-\langle\sigma(\mathrm{Xe@cage})\rangle]/[1-\sigma(\text{free Xe atom})]. \quad (7)$$

Figure 6 shows a comparison between the Monte Carlo average Xe chemical shift in cage A at 300 K and the experimental Xe NMR spectrum in $(CHCl_2)_2$ solution. The direction of the chemical shift relative to the free atom (gas phase peak, not shown in the experimental spectrum) is correctly predicted. The agreement of the calculated average with the magnitude of the experimental chemical shift is reasonably good, somewhat too deshielded as expected. The average values calculated here using the B3LYP shielding functions could be too deshielded by about 15% since we have found that B3LYP values for the Xe shielding in Xe–rare gas pairs are about 15% too large (too deshielded). If the same fractional error holds for Xe in the cryptophane cages, that is, had we multiplied the DFT/B3LYP shielding functions by the factor 0.85 that brought Xe–rare gas values into agree-

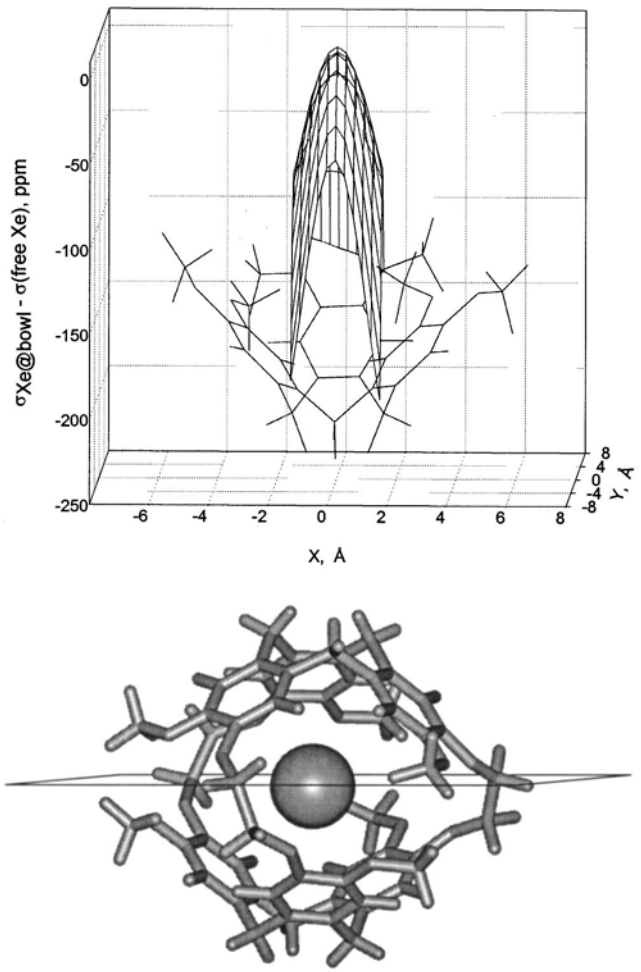

FIG. 5. The shielding surface for Xe inside the cryptophane-A cage is illustrated in part, where the isotropic shielding values are shown (relative to free Xe atom) for those Xe locations in the plane of the equator of the cage.

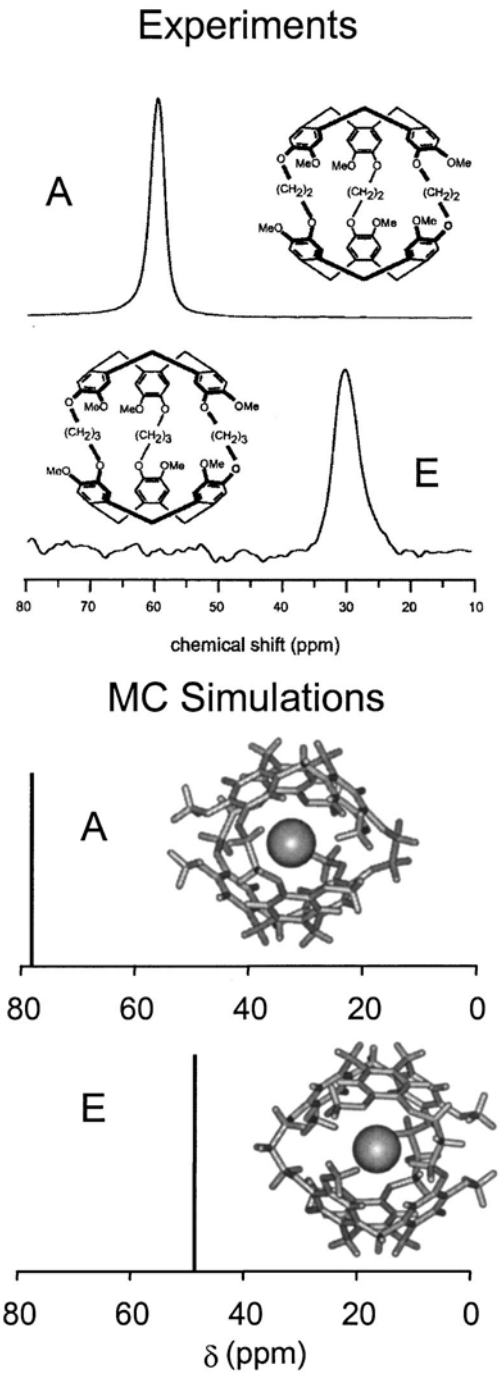

FIG. 6. Comparison between the Monte Carlo average Xe shielding in cryptophane-A and -E and the experimental Xe NMR spectra of Pines *et al.* Experimental spectra were reproduced from Ref. 19, with permission from the Proceedings of the National Academy of Sciences.

ment with experimental gas phase measurements,[28] then the average Xe shielding corrected for this overestimation would fall nearly exactly on the observed peak.

With the same shielding functions and the same potential functions, we carried out the Monte Carlo averaging of the Xe shielding for Xe inside cryptophane-E. The dependence of the Xe shielding upon the distance of Xe from the cage atoms should lead to a smaller average chemical shift for Xe in the larger cryptophane-E compared to Xe in the smaller cryptophane-A. In Fig. 6 we show the results of the Monte Carlo simulations for cage E compared with the experimental spectrum in $(CHCl_2)_2$. We see that the relative chemical shifts of Xe in cages A and E are reproduced quite well. The experimental separation between the two Xe signals is reported as 30 ppm,[19] while our calculated value for this difference is 29.5 ppm at 300 K.

Using the same shielding functions and the same potential functions, we can calculate the average Xe shielding in cryptophane-A as a function of temperature. The calculated results are compared with experiments in Fig. 7 (see supplementary table for numerical values).[35] The cage is assumed to be static and the entire temperature dependence arises from the different sampling of Xe locations within the cage. We see that the Xe chemical shift increases with increasing temperature. This behavior is associated with the Xe being able to sample the repulsive regions of the Xe–C (or O) potential with increasing probability at higher temperatures. These are the regions of greater deshielding for all cage atoms, as seen in Fig. 5. Thus, by being able to approach closer to the cage atoms at higher temperatures, the Xe becomes more deshielded on average. This trend in Xe chemical shifts with increasing temperature is characteristic of small pores. A single Xe atom in larger pores such as the supercages in

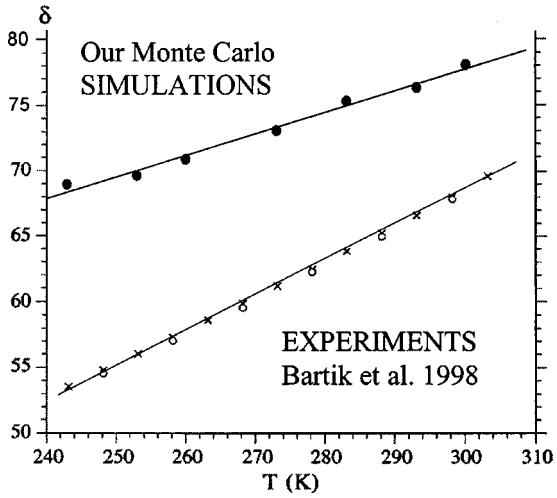

FIG. 7. Average Xe shielding in cryptophane-A cage as a function of temperature. Experimental data were reproduced from Ref. 37, with permission. Average Xe chemical shift values from our simulations (●), experimental values (×) for $n_{Xe}/n_{cage}=0.46$ and (○) for $n_{Xe}/n_{cage}=2.1$.

zeolite NaY or NaA shows the opposite trend.[17,36] The temperature dependence over the small range of temperatures of the experiment appears to be linear in both experiments and our calculations. However, we observe a slight curvature with leveling off at the lower temperature end. In Fig. 7, we note the overall displacement by about 15% in absolute Xe chemical shifts for reasons already mentioned. Nevertheless, our calculated averages compare favorably with the experimental temperature dependence reported by Bartik *et al.*[37] We obtain the correct sign of the temperature coefficient and close to the right magnitude. Our calculated temperature coefficient of the chemical shift (the slope of the line in Fig. 7) is smaller than that obtained experimentally. We do not expect to reproduce the observed temperature dependence accurately since some of the observed temperature dependence is undoubtedly due to fluxional changes of the cage itself, leading to distortions that change the shape of the internal volume explored by the Xe atom, which is something we have not included in our Monte Carlo simulations. We consider the effect of such cage distortions in Sec. IV.

When the hydrogen atoms of the cage are replaced by deuterium atoms, the average Xe shielding is expected to change. This isotope dependence of the Xe chemical shift can be calculated in a comprehensive MD simulation in which the cage atoms as well as the Xe are permitted to move, with no change in the potential parameters, only a change in masses. Deuterium atoms have vibrational amplitudes that are smaller than that of hydrogen atoms in C–D stretches compared to C–H stretches. Deuterium atoms also have smaller vibrational amplitudes in other modes such as bond angle deformations. As they vibrate, the hydrogen atoms sweep out a larger space around their equilibrium position than do the deuterium atoms. The net effect is that the Xe can get closer to the cage atoms when the hydrogens are replaced by the heavy isotope. MD simulations in which all atoms are permitted to move, using a good force field for the cage atoms, can provide these effects. In lieu of such MD simulations that include fluxional as well as local mode vibrational motions of the cage, we mimic this dynamic isotope effect by simply using a somewhat shorter r_0 for Xe–D than for Xe–H and carry out the Monte Carlo simulations as before, keeping the coordinates of the cage atoms unchanged. A small difference in r_0 for the Xe–H and the Xe–D function may alter the one-body distribution function sufficiently to reproduce the observed Xe isotope shifts induced by deuteration of the linker and methoxy hydrogens. By making the value of the Xe–D r_0 0.07 Å shorter than for Xe–H, without changing the well depth, we allow a larger space swept out by the lighter hydrogen atom than the deuterium atom. The results are shown in Table II and Fig. 8. We ''deuterated'' the OCH_2CH_2O bridges and the OCH_3 groups separately so as to generate the isotopomers for which the Xe NMR spectra were observed. The canonical Monte Carlo simulations of Xe inside the successively deuterated cryptophane-A cage provide the nearly additive isotopically induced Xe chemical shifts. We compare these with the isotopic shifts that were reported by Brotin *et al.* in successively deuterated cryptophane cages.[18] It was found experimentally that the per-D isotope effect is smaller for the methoxy hydrogens than for the linker hydrogens. This difference arises from the relative accessibility to Xe of these types of hydrogen sites, and we do find in our simulations that the per-D isotope effect is smaller for the methoxy hydrogens than for the linker hydrogens, as seen in Table II. The excellent agreement between our calculations and the experimental results implies that our shielding response functions and potential functions are adequate, and the coordinates we have derived for the average solution structure of the cryptophane-A cage are reasonably accurate, especially with respect to the OCH_3 and $O(CH_2)_2O$ portions. We reproduce the sign of the isotope shifts, the relative magnitudes for the two types of hydrogen positions, and the absolute magnitudes of the isotopic shifts.

TABLE II. Monte Carlo average Xe chemical shifts in deuterated cryptophane-A (in ppm) relative to the parent all-proton cryptophane-A. Positions of deuterium substitution are shown in Fig. 8. Experimental values are from Ref. 18.

Cryptophane-A isotopomers[a]	Isotope shifts (ppm) Calculated	Isotope shifts (ppm) Experimental
1 OCH_2CH_2O all; OCH_3 all,	0.0	0.0
3 OCD_2CD_2O all; OCH_3 all	0.55	0.58
OCH_2CH_2O all; OCD_3 all	0.53	0.61
6 OCD_2CD_2O all, OCD_3 all	1.12	1.20
per D in OCD_3	0.029	0.034
per D in OCD_2CD_2O	0.046	0.048

[a]Isotopomer numbering system (1,3,6) follows from Ref. 18.

Finally, for a more comprehensive study, we consider the dependence of the Xe chemical shift on the length of the linker groups that connect the top cyclotriveratrylene bowl to the bottom bowl. Cryptophane-A has three $O(CH_2)_2O$ bridges, whereas cryptophane-E has three $O(CH_2)_3O$ bridges. Descriptive designations would be cryptophane-222 and -333, respectively, as seen in Fig. 1. To find the best atomic coordinates for these symmetrical cryptophanes, we had done quantum mechanical geometry optimization of the

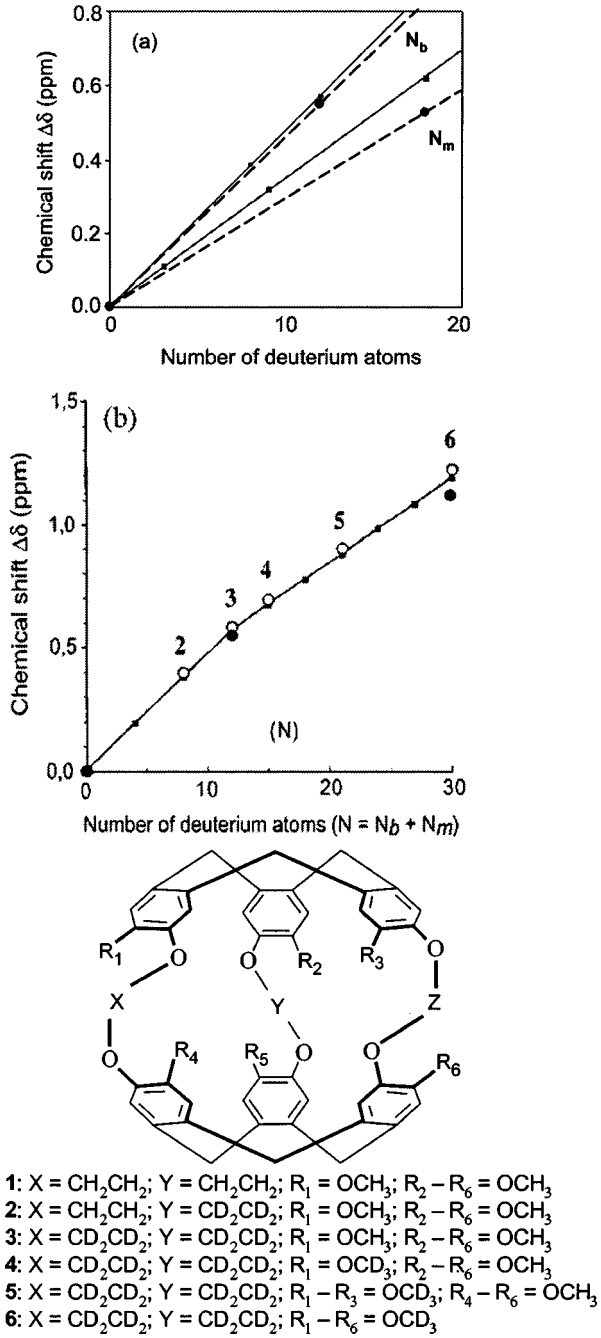

FIG. 8. Canonical Monte Carlo simulations of Xe inside the successively deuterated cryptophane-A cage yields additive isotopically induced Xe chemical shifts. Experimental data of Brotin *et al.* were reproduced from Ref. 18, with permission from the American Chemical Society. Symbols for average Xe chemical shift values from our simulations (●), experimental values (•), (○); *m* stands for methoxy, and *b* for bridge (linker) hydrogens.

22 fragment for A and the 33 fragment for E, in which cases the rigid parts of the bowls were anchored by the x-ray data and the linker conformations had already been obtained by quantum-mechanical geometry optimization. We choose not to use this procedure with the 223 and 233 cages since the lower symmetry of these cages (C_2) precludes knowledge of the precise tilt of the two bowls; no x-ray data are available for these mixed-linker cages. Instead we found the minimum energy structures of cryptophane-223 and -233 by doing molecular dynamics of each full cage with an encapsulated guest in a simulation box of $(CHCl_2)_2$ liquid solvent to find the optimum geometry of each, as described in Sec. II. The important parameter is the pole-to-pole distance that governs, as in cryptophane-A and -E, the volume of the space between the more rigid bowl portions. The molecular mechanics MD simulations that we carried out do provide a systematically increasing pole-to-pole average distance in going from 222 to 333 in this series. Furthermore, in the 223 and 233 cages, we find the bowls in a clam-like attitude toward each other, somewhat pinched together along the short linkers. This is in agreement with the SPIROE results of Desvaux *et al.* on the cryptophane-233 cage in solution in $(CHCl_2)_2$, in which there is evidence of the Xe interacting through space with the aromatic protons and with the protons of the $O(CH_2)_2O$ linker, but no signal corresponding to an interaction with the $O(CH_2)_3O$ linkers.[38] Having found the optimum geometries for the cages at this level of optimization, we could refine the coordinates of the OCH_3 groups by quantum-mechanical geometry optimization of the 2/3 of each cage as we had done for the A and E cages. We chose not to do this because the accuracy of the starting geometry information (orientations and separation of the opposite aromatic rings) in the hybrid cages is not as high as in the symmetrical cages. Thus, we adopt the molecular mechanics MD-optimized minimum energy structures for the cryptophane-223 and -233 for our static cage coordinates to be used in the Monte Carlo simulations.

The one-body distribution function for the Xe in cryptophane-223 and -233 resulting from the Monte Carlo simulations is shown in comparison with that for Xe in cryptophane-A in Fig. 9. The results were obtained using the same potential functions for Xe in all cages. It is clearly evident that the Xe atom does have a higher probability of being found close to the $O(CH_2)_2O$ linker(s) and a smaller probability of being found close to the $O(CH_2)_3O$ linker(s) in the unsymmetrical cages. This is in agreement with the SPIROE experiments of Desvaux *et al.* for cryptophane-233.[38] The highest probability of finding Xe in the hybrid cage is off center and closer to the shorter linker. When the Xe atom is off center, the clam-like attitude of the two cyclotriveratrylene bowls in cryptophane-233 permits the Xe atom to have shorter distances to the aromatic ring protons and to the protons of the shorter linker in comparison to the longer linkers, in contrast to Xe in the cryptophane-A or -E, in which the three linkers are identical.

The results of doing Monte Carlo averaging of Xe in the four related cryptophane cages, obtained using the same potential functions and the same shielding functions (changing only the coordinates of the cage atoms), are shown in Fig. 10. We see that the systematic progression of decreasing Xe chemical shift in going across the types 222, 223, 233, 333[18,19,39] is reproduced very well. Furthermore, our theoretical predictions for the numerical average Xe chemical shifts are in reasonably good agreement with the experimental data for all four cages, as shown in Table III. The separation of 30 ppm observed by Spence *et al.* between Xe at cryptophane-A and -E[19] is reproduced (29 ppm). Finally, the separation of the peaks, 13 ppm between Xe in cryptophane-223 and Xe in

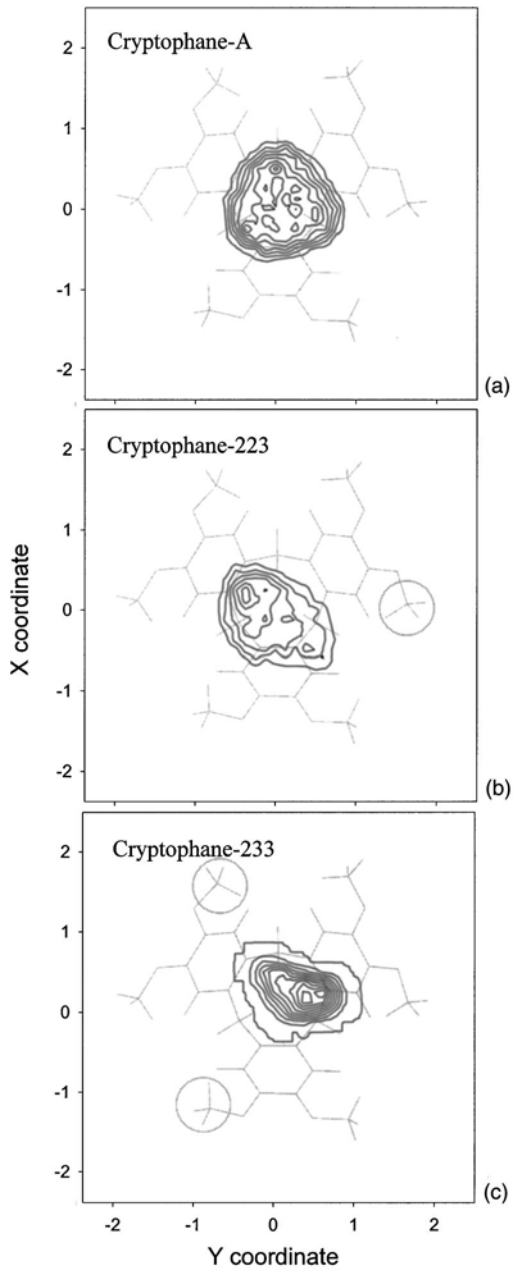

FIG. 9. The one-body distribution of Xe atom in (a) cryptophane A, (b) cryptophane-233, and (c) cryptophane-233, resulting from Monte Carlo simulations. The asymmetry of the one-body distribution in the hybrid cages may be contrasted with the symmetrical distribution in the 222 (cryptophane-A) cage. Overlaid on the contours are the cyclotriveratrylene structures which still have OCH_3 groups instead of the $O(CH_2)_nO$ linkers, for the purpose of orientation. The locations of the longer $O(CH_2)_3O$ linkers in the hybrid cages are indicated with circles around the replaced OCH_3 groups.

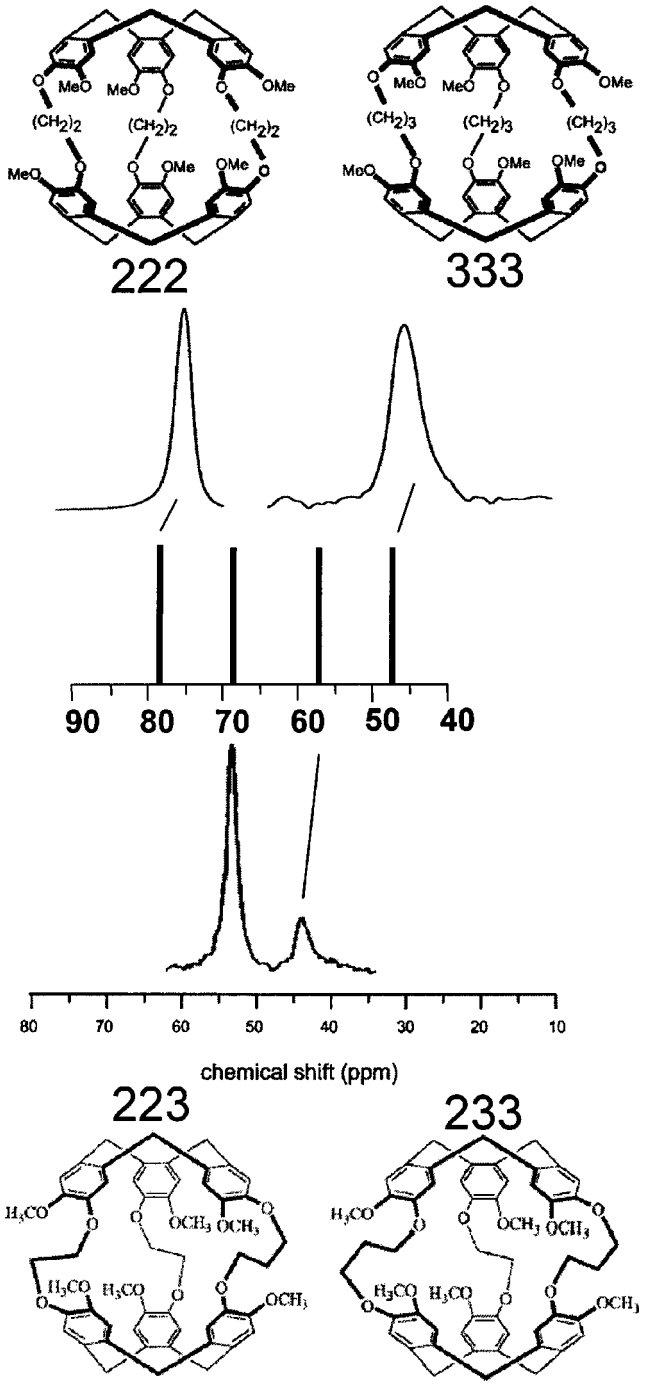

FIG. 10. The experimental and calculated average Xe chemical shifts associated with progressive linker changes leading from cryptophane-A to cryptophane-E. Cryptophane-A linkers consist of three $O(CH_2)_2O$ linkers, designated as 222, and cryptophane-E is designated as cryptophane-333. Cryptophane-223 and cryptophane-233 have mixed linker groups. Experimental spectra were reproduced from Ref. 19, with permission from the Proceedings of the National Academy of Sciences and Ref. 39, with permission from the European Journal of Organic Chemistry. For direct comparison, chemical shift scales (in ppm relative to free Xe atom) are kept the same for all experimental and calculated spectra.

cryptophane-233 observed by Brotin and Dutasta at 293 K,[39] is also reproduced in our work (12 ppm at 300 K).

IV. DISCUSSIONS

In our simulations of Xe in cryptophane cages, we find general trends of Xe chemical shifts with cage size and shape which are consistent with the known behavior of Xe chemical shifts when comparing similarly constituted cavities and channels. Given the universal shape of the Xe shielding response function proposed by us in 1982 and verified by *ab initio* calculations on Ar–Ar,[40] the dependence of the average Xe chemical shift on cage size found in this work follows from the fact that a smaller cage provides the Xe atom with many more atoms at short distances to evoke a large quan-

TABLE III. Monte Carlo average Xe chemical shifts inside different cryptophane cages, compared with experimental data in solution in $(CDCl_2)_2$ (ppm) relative to free Xe atom.

Cryptophane cage	Calculated	Experimental	Reference
222 (A)	69.62 at 253 K	~60[a]	19
	73.72 at 278 K	63.0 at 278 K	18
	76.35 at 293 K	~68 at 293 K[b]	39
	78.09 at 300 K	other data shown in Fig. 7	37
223	60.95 at 238 K	~42 at 238 K[b]	39
	67.18 at 278 K	~53 at 278 K[b]	39
	69.00 at 293 K	~60 at 293 K[b]	
	69.33 at 300 K		
233	49.00 at 238 K	~32 at 238 K[b]	39
	54.43 at 278 K	~43 at 278 K[b]	39
	56.67 at 293 K	~47 at 293 K[b]	
	57.26 at 300 K		
333 (E)	43.53 at 253 K	~30[a]	19
	45.28 at 278 K		
	48.58 at 300 K		

[a]From published spectra at an unspecified temperature (Ref. 19).
[b]From published spectra (Ref. 39).

tum mechanical deshielding response. The calculated absolute Xe chemical shifts shown in Fig. 10 for the four types of cages are individually in good agreement with experiment. The relative chemical shifts are in excellent agreement with experiment.

The effect of isotopic substitution is very well represented in the present work. The isotope effects are also an exquisite measure of the dependence of the average Xe chemical shift on cage size. The frequencies of C–H stretches, CH_2 wags, scissoring motions, and other vibrational modes involving the hydrogen atoms of the cage are much greater than the rate at which the Xe moves around in the cage, so that the vibrations can be considered, in a Born–Oppenheimer separation, as effectively decoupled from Xe displacements within the cage. For this reason, we have used average hydrogen diameters for the light and heavy isotopes to reflect the relative amplitudes of motion during vibrations as a means of including the mass effect. All other data, atomic coordinates, potential functions, and shielding functions remain unchanged. The per-D shift of the Xe is found to be smaller for deuterium substitution at the OCH_3 groups than for substitution at the OCH_2CH_2O groups because the OCH_3 groups are farther away form the center of the cage in the quantum-mechanically optimized structure of cage A. As seen in Fig. 8, our calculated results agree with experiment in the direction of the isotope shift, in the relative magnitudes of OCH_3 versus OCH_2CH_2O deuterium substitution, and also in the absolute magnitudes of the isotopic shifts. Therefore, we have a quantitative understanding of the observed isotope shifts in this case.

We find the temperature dependence of Xe chemical shift in cryptophane-A (see Fig. 7) to be consistent with that of a crowded environment, increasing with increasing temperature, as opposed to a zeolite with large cages, such as zeolite NaY, in which the temperature dependence is quite the opposite (decreasing with increasing temperature).[36] The cryptophane-A cage is sufficiently small so that there appears to be a single potential energy minimum located at the center of the cage, rather than a spherical shell trough more typical of a larger cage. As the temperature increases, the one-body distribution function spreads out into regions of high potential energy, which correspond to regions of greater deshielding. Inclusion of contributions from Xe locations with greater deshielding leads to larger average Xe chemical shifts. With Monte Carlo simulations using a static cage, we reproduce the sign of the temperature dependence and nearly the correct magnitude. The simulations also provide the temperature dependence of the Xe chemical shift in the cages 223, 233, and 333 (E), shown in Table III. The Xe chemical shifts read off from the published experimental spectra are given in Table III. The observed increase of the Xe chemical shift with increasing temperature in the hybrid cages 223 and 233[39] is well reproduced by the theoretical calculations in terms of the sign of the temperature dependence. The change of the Xe chemical shift with temperature is in the same direction as was observed and calculated for cryptophane 222 (A).[37] The magnitude of the temperature coefficient that we calculated is smaller than that observed experimentally in cryptophane-223 and -233.

The cage is fluxional in solution, permitting the Xe atom to exchange between the solution and the cage, although the exchange is sufficiently slow that two distinct peaks can be observed in the ^{129}Xe NMR spectrum: one for Xe in the solvent and another for Xe inside the cage.[37] This exchange is the mechanism by which the spin polarization of the ^{129}Xe inside the biosensor cage is continuously replenished from the polarization of Xe in the solution phase.[19] The fluxional dynamics of the real cryptophane cage in solution provides instantaneous various-shaped cages that the Xe atom is able to explore fully. By doing Monte Carlo averaging in several cage structures that have been extracted out of molecular dynamics simulations, we find that each such transient cage structure can contribute Xe chemical shift values that differ by a few ppm from the average chemical shift using a static cage of average structure. The range of transient structures must change with temperature as well. Doing Monte Carlo simulations in the full range of structures would be prohibitive, but the direction of the corrections to the temperature dependence is clearly toward increasing the temperature coefficient and moving our calculated temperature dependence closer to the experiment.

We placed the cage with the starting coordinates at the minimum energy structure into a molecular dynamics trajectory. We used the same force field as described in Sec. II and picked out several snapshots of the cage. For these small number of distorted static cages, we carried out Monte Carlo simulations as before, using the same set of shielding functions and potential functions. We find that the average Xe chemical shifts in these distorted cages can vary by as much as 3.5 ppm, which indicates that any changes in geometry associated with cage fluxional motions do change the average Xe chemical shift. We find that a distortion leading to a less symmetrical cage than the one we have used as our average optimum structure in solution can lead to a more

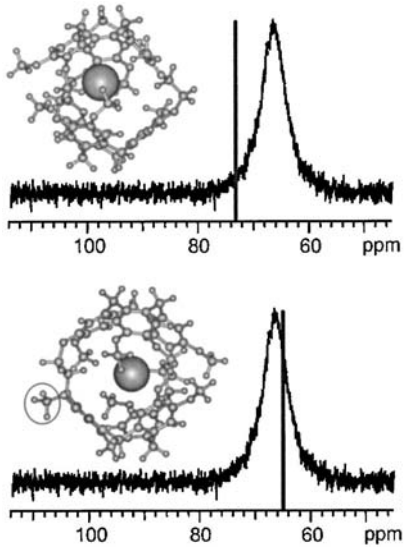

FIG. 11. Changes in MC average Xe chemical shifts upon hypothetical deformations of the cryptophane-A cage: (bottom) in which one OCH_3 (circled) is stretched outward from the center, and (top) in which the cage is flattened on one side. The experimental spectra correspond to that of undeformed cryptophane-A; the line spectra show the calculated Xe chemical shift displacements which result from the Monte Carlo simulations in the mechanically deformed cryptophane-A cages.

deshielded average shielding relative to the symmetrical cage. The reason for this is clearly seen in the nonlinear Xe shielding function. Despite the unfavorable Boltzmann factor, the steep deshielding that occurs with decreasing distances of the Xe atom to the cage atoms leads to disproportionately large contributions at any temperature. Thus, for the same change in volume, compression of the cage leads to a larger Xe chemical shift than expansion of the cage. Therefore, Monte Carlo simulations in a static cage at the minimum energy structure leads to a smaller Xe chemical shift than a true dynamic averaging of the chemical shift.

In the application of functionalized Xe as a biosensor, a Xe atom is introduced into a cryptophane-A derivatized with a tether, which in turn is connected to a molecular fragment that is capable of binding to a specific protein. Cage distortion may be relevant to this biosensor application. For example, what if the derivatization of the cryptophane cage by attaching a tether causes the average geometry of the cage to change in the manner of replacing one OCH_3 with an outfacing (away from the center of the cage) functional group? We can mimic this tether effect with Monte Carlo averaging in a static cage that has been subjected to a specific mechanical distortion, that is, one OCH_3 group is systematically moved away from the center of the cage compared to the optimum geometry structure. Since this hypothetical distortion involves no change in electronic structure, then we can use the same shielding functions and the same potential functions to carry out the Monte Carlo averaging. We find the consequence of this mechanical change in cage structure is to change the average shielding to a less deshielded value by 0.46 ppm. These results are shown in Fig. 11, where the theoretical Xe chemical shift difference between the undeformed and deformed cages is superimposed on the cryptophane-A experimental spectrum. The direction of the change, that is, to somewhat smaller chemical shift values, may be compared with the Xe chemical shifts found in the cryptophane-A dimer, in which two cryptophane A cages are chemically linked by having two OCH_3 groups, one from each cage be replaced by one $O-(CH_2)_{10}-O$ linker that connects the two cages to each other,[41,42] when this information becomes available.

The premise is, of course, an oversimplifying one, that there is no change in the electronic structure of the cage atoms. On the contrary, upon derivatizing the cryptophane-A with various functional groups toward increasing the solubility of the cage in aqueous solution, it is found experimentally that the Xe invariably shifts toward lower chemical shifts (less deshielded values) relative to Xe in the parent cryptophane-A by about 1–15 ppm, depending on the derivative.[43,44] Our model of one OCH_3 mechanically directed away from the cage center leads to the same direction of chemical shift change as upon introduction of a tether to the cage. However, it fails as a model for the tethered cryptophane-A cage; the magnitude of the effect we found by mechanical changes on the cage is too small compared to the 1–15 ppm shift to lower chemical shift values observed for various tethers.[19,43,44] We will, of course, need the electronic effects on the cage from the tether functional groups, some of which are highly polar. We defer discussion of such simulations to a later paper.[45]

In the first demonstration of Xe functionalized with a tethered cryptophane-A cage, the protein (avidin) was recognized through the binding of the biotin group attached to the end of the tether. In this example, the Xe chemical shift increased (toward more deshielding) by about 2.3 ppm upon binding, thus providing a biosensor capability.[19] To mimic the effect on the Xe chemical shift arising from a mechanical deformation of the cryptophane cage such as might occur upon being flattened against a protein surface, we carried out Monte Carlo simulations in a deformed cage, using the same shielding functions and potential functions. The coordinates of the deformed cage in this case were found by doing a molecular dynamics simulation of the cryptophane-A with encapsulated $CHCl_3$ in $(CHCl_2)_2$ solvent, just as described in Sec. II, except that a polymer membrane was incorporated into the simulation box. The polymer was first equilibrated in vacuum. Then the solvent was introduced and the polymer was permitted to relax in the liquid solvent before the cage with encapsulated $CHCl_3$ was introduced. In order to flatten the cage against the polymer membrane, five additional solvent molecules were introduced, leading to a 15% increase in the solvent number density compared to its normal density at room temperature. This resulted in a somewhat flattened cage. In Monte Carlo calculations parallel to those described above for the outstretched OCH_3 group, we have found that an increase of 3.5 ppm in the average Xe chemical shift could easily be accounted for by using a static cage with a distortion of this type. In the top part of Fig. 11, the theoretical Xe average chemical shift difference between the deformed and undeformed cage is shown as a spectral line superimposed on the experimental spectrum. That is, any mechanical cage distortions which tend to decrease the ratio of the internal volume to the internal surface area of the cage

leads to an increased Xe chemical shift. This is easily understood in terms of the deformation away from the nearly spherical internal space of the cryptophane cage, that is, away from the maximum internal volume to surface ratio, which leads to increased short-distance contacts of Xe with the cage atoms, which in turn leads to increased Xe deshielding. Thus, if the cryptophane cage becomes mechanically distorted upon being held close to the protein surface, the expected Xe chemical shift change upon binding is toward a more deshielded Xe average; this is in accord with what is observed experimentally.

In our simulations of average Xe shielding response to these two types of cage distortions, it has been assumed that there are no accompanying electronic factors. Electronic factors can lead to either sign of the Xe shielding change since electronic factors affect both the intrinsic Xe shielding response and also the potential functions, by withdrawing or enhancing electron density of the cage atoms. On the other hand, the mechanical cage distortions that we have imposed in Fig. 11, followed by Monte Carlo simulations using the same shielding functions and the same potential functions, merely changes the Xe one-body distribution function within the cage and the pair distribution functions of Xe with individual cage atoms. The modified Xe distribution functions provide different averages via modified weighting of the unchanging Xe site shielding functions that we are using for all the simulations in this paper, all of which have the general intrinsic dependence on the Xe–cage atom distance, which is a pronounced deshielding toward shorter distances.

In Fig. 11, we comment on the Xe chemical shifts for functionalized Xe in biosensor applications by investigating possible mechanical distortions of the cage resulting from: (a) having a long tether that is strongly interacting with water in the aqueous solutions used for the applications, mimicked by Xe averaging within a cage having an outstretched OCH_3 group and (b) flattening of the cage against some macromolecular surface. It appears that mechanical cage deformations alone can affect the averaging of the Xe shielding in directions that are in complete agreement with experimental results, without taking into account the inevitable electronic structure changes that the cage atoms undergo upon functionalization. Actual magnitudes of Xe shifts observed upon derivatization of the cage with various tethers[44] are much greater than can be accounted for by mere mechanical deformations of the cryptophane cage.

V. CONCLUSIONS

We have reproduced the observed Xe chemical shift for Xe@cryptophane-A relative to the free Xe atom. We find the correct sign and magnitude of the Xe chemical shift. We have reproduced the Xe chemical shift for Xe in the larger cryptophane-E cage and we find the correct relative Xe chemical shift of about 30 ppm between these two cages. The chemical shift relative to the free Xe atom is smaller in the larger cryptophane-E cage than the A cage for the same reason that, for similarly constituted zeolite cavities, Xe chemical shifts are found to be smaller for the larger cavities. The general nature of the Xe intermolecular shielding function (becoming more deshielded with closer approach of a neighbor atom) and the general nature of one-body distribution functions in concave spaces together lead to this correlation of Xe chemical shift with cavity size for similarly constituted cavities (similar Xe shielding functions).

The temperature dependence of the Xe chemical shift in the cryptophane-A cage arises because the one-body distribution function of the Xe atom becomes less sharply peaked at higher temperatures, where the more favorable Boltzmann factor affords a higher probability of finding the Xe closer to the cage atoms. At close approach, the deshielding of the Xe is more pronounced for each type of cage atom. We have reproduced the sign of the observed temperature coefficient. This direction of temperature dependence is expected for a single Xe in a small cavity.[34] The order of magnitude of the observed temperature coefficient is also reproduced in our calculations, even without permitting a distortion of the cage. A more complete averaging using molecular dynamics should provide a more accurate answer, provided that a reasonably realistic force field can be constructed for the cryptophane cage.

We have completely reproduced the changes in the Xe chemical shifts upon successive deuteration of the cryptophane cage by making the effective volume occupied dynamically by the deuterium atoms slightly smaller than that of the hydrogen atoms, in which case the general nature of the Xe intermolecular shielding functions provides the correct sign of the Xe shift upon deuteration. The difference between the H- and D-containing cages is that the greater vibrational amplitude of the C–H compared to C–D effectively restricts the Xe one-body distribution functions to a slightly smaller volume of space in the H_n–cryptophane-A than in D_n–cryptophane-A.

Finally, we find that certain types of mechanical cage distortions can lead to smaller or larger Xe chemical shifts. A cage distortion that pulls the OCH_3 out and farther away from the center of the cage can lead to a smaller Xe chemical shift in the Monte Carlo average, such as that which may be found upon derivatization with a functional group that pulls the former $O–CH_3$ group away from the center of the cage on average. On the other hand, mechanical cage distortions that lead to a less symmetrical, flattened cage structure, such as may occur upon attaching the cage to the surface of a macromolecule, can lead to a larger Xe chemical shift. These effects of hypothetical mechanical cage distortion on the Xe chemical shifts present an incomplete picture in that we have not considered the electronic effects of chemical derivatization of the cage. Nevertheless, they provide insight into Xe chemical shift changes that result from changes in the average structure of the cage, toward a general understanding of biosensor applications of Xe in cages.

ACKNOWLEDGMENTS

This research was funded by the National Science Foundation (Grant No. CHE-9979259), for whose continued support we are very grateful. This work has been motivated and inspired by the biosensor applications proposed by Alex Pines, David Wemmer, and their research groups. C.J.J. is grateful to the Miller Research Foundation for a Visiting Research Professorship at University of California—Berkeley,

and for the discussions with Megan Spence, Seth Rubin, Janette Ruiz, and Alex Pines about the development of Xe in cages as biosensors. We also thank Professor Dutasta for kindly providing us with the x-ray data for cryptophane-A prior to publication.

[1] B. C. Schoenborn, H. C. Watson, and J. C. Kendrew, Nature (London) **207**, 28 (1965).
[2] Y. Montet, P. Amara, A. Volbeda, X. Vernede, E. C. Hatchikian, M. J. Field, M. Frey, and J. C. Fontecilla-Camps, Nat. Struct. Biol. **4**, 523 (1997).
[3] P. Wentworth, Jr. *et al.*, Science **293**, 1806 (2001).
[4] D. A. Whittington, A. C. Rosenzweig, C. A. Frederick, and S. J. Lippard, Biochemistry **40**, 3476 (2001).
[5] A. Bifone, Y. Q. Song, R. Seydoux, R. E. Taylor, B. M. Goodson, T. Pietrass, T. F. Budinger, G. Navon, and A. Pines, Proc. Natl. Acad. Sci. U.S.A. **93**, 12932 (1996).
[6] J. Wolber, A. Cherubini, M. O. Leach, and A. Bifone, Magn. Reson. Med. **43**, 491 (2000).
[7] S. D. Swanson, M. S. Rosen, K. P. Coulter, R. C. Welsh, and T. E. Chupp, Magn. Reson. Med. **42**, 1137 (1999).
[8] G. Duhamel, P. Choquet, E. Grillon, L. Lamalle, J. L. Leviel, A. Ziegler, and A. Contantinesco, Magn. Reson. Med. **46**, 208 (2001).
[9] J. Wolber, D. J. O. McIntyre, L. M. Rodrigues, P. Carnochan, J. R. Griffiths, M. O. Leach, and A. Bifone, Magn. Reson. Med. **46**, 586 (2001).
[10] S. M. Rubin, S. Y. Lee, E. J. Ruiz, A. Pines, and D. E. Wemmer, J. Mol. Biol. **322**, 425 (2002).
[11] J. A. Ripmeester, C. I. Ratcliffe, and J. S. Tse, J. Chem. Soc., Faraday Trans. 1 **184**, 3731 (1988).
[12] E. G. Derouane and J. B. Nagy, Chem. Phys. Lett. **142**, 200 (1987).
[13] J. Demarquay and J. Fraissard, Chem. Phys. Lett. **136**, 314 (1987).
[14] J. A. Ripmeester and D. W. Davidson, J. Mol. Struct. **75**, 67 (1981).
[15] D. W. Davidson, Y. P. Handa, and J. A. Ripmeester, J. Phys. Chem. **90**, 6549 (1986).
[16] I. L. Moudrakovski, C. I. Ratcliffe, and J. A. Ripmeester, J. Am. Chem. Soc. **123**, 2066 (2001).
[17] C. J. Jameson, A. K. Jameson, R. Gerald II, and A. C. de Dios, J. Chem. Phys. **96**, 1676 (1992).
[18] T. Brotin, A. Lesage, L. Emsley, and A. Collet, J. Am. Chem. Soc. **122**, 1171 (2000).
[19] M. M. Spence, S. M. Rubin, I. E. Dimitrov, E. J. Ruiz, D. E. Wemmer, A. Pines, S. Q. Yao, F. Tian, and P. G. Schultz, Proc. Natl. Acad. Sci. U.S.A. **98**, 10654 (2001).
[20] A. Collet, in *Comprehensive Supramolecular Chemistry*, edited by J. L. Atwood, J. E. D. Davis, D. D. MacNicol, and F. Vogtle (Pergamon, New York, 1996), Vol. 2, Chap. 11, pp. 325–365.
[21] J. P. Dutasta (private communications).
[22] A. Varnek, S. Helissen, and G. Wipff, J. Comput. Chem. **19**, 820 (1998).
[23] J. Canceill, A. Collet, G. Gottarelli, and P. Palmieri, J. Am. Chem. Soc. **109**, 6454 (1987).
[24] M. Luhmer, B. M. Goodson, Y. Q. Song, D. D. Laws, L. Kaiser, M. C. Cyrier, and A. Pines, J. Am. Chem. Soc. **121**, 3502 (1999).
[25] J. Canceill, M. Cesario, A. Collet, J. Guilhem, L. Lacombe, B. Lozach, and C. Pascard, Angew. Chem., Int. Ed. Engl. **28**, 1246 (1989).
[26] K. Wolinski, J. F. Hinton, and P. Pulay, J. Am. Chem. Soc. **112**, 8251 (1990).
[27] A. C. de Dios and C. J. Jameson, J. Chem. Phys. **107**, 4253 (1997).
[28] C. J. Jameson, D. N. Sears, and A. C. de Dios, J. Chem. Phys. **118**, 2575 (2003).
[29] D. N. Sears and C. J. Jameson, J. Chem. Phys. **118**, 9987 (2003).
[30] T. Brupbacher, J. Makarewicz, and A. Bauder, J. Chem. Phys. **101**, 9736 (1994).
[31] C. J. Jameson, A. K. Jameson, P. Kostikin, and B. I. Baello, J. Chem. Phys. **112**, 323 (2000).
[32] G. C. Maitland, M. Rigby, E. B. Smith, and W. A. Wakeham, *Intermolecular Forces, Their Origin and Determination* (Clarendon, Oxford, 1981).
[33] G. Liuti, F. Pirani, U. Buck, and B. Schmidt, Chem. Phys. **126**, 1 (1988).
[34] D. Stueber and C. J. Jameson, J. Chem. Phys. (to be published).
[35] See EPAPS Document No. E-JCPSA6-119-304347 for Table of values. A direct link to this document may be found in the online article's HTML reference section. The document may also be reached via the EPAPS homepage (http://www.aip.org/pubservs/epaps.html) or from ftp.aip.org in the directory /epaps/. See the EPAPS homepage for more information.
[36] A. Laboriau, T. Pietrass, W. A. Weber, B. C. Gates, and W. L. Earl, J. Phys. Chem. B **103**, 4323 (1999).
[37] K. Bartik, M. Luhmer, J. P. Dutasta, A. Collet, and J. Reisse, J. Am. Chem. Soc. **120**, 784 (1998).
[38] H. Desvaux, J. G. Huber, T. Brotin, J. P. Dutasta, and P. Berthault, ChemPhysChem **2003**, 384.
[39] T. Brotin and J. P. Dutasta, Eur. J. Org. Chem. **2003**, 973.
[40] C. J. Jameson and A. C. de Dios, J. Chem. Phys. **97**, 417 (1992).
[41] M. Darzac, T. Brotin, D. Bouchu, and J. P. Dutasta, Chem. Commun. (Cambridge) **2002**, 48.
[42] T. Brotin, J. Lawrence, and J. P. Dutasta, International Symposium on Xenon NMR of Materials, XEMAT 2003, La Colle-sur-Loup, France, May 29–31, 2003.
[43] E. J. Ruiz, M. M. Spence, S. M. Rubin, D. E. Wemmer, A. Pines, N. Winssinger, F. Tian, S. Q. Yao, and P. G. Schultz, Proceedings 43rd Experimental NMR Conference, Asilomar, CA, April 14–19, 2002.
[44] E. J. Ruiz (private communications).
[45] C. J. Jameson and D. N. Sears (unpublished).